

University of Nebraska - Lincoln

DigitalCommons@University of Nebraska - Lincoln

---

Peter Dowben Publications

Research Papers in Physics and Astronomy

---

6-1-2020

## Surface termination and Schottky-barrier formation of $\text{In}_4\text{Se}_3(001)$

Archit Dhingra

University of Nebraska–Lincoln, archit.dhingra@huskers.unl.edu

Pavlo V. Galiy

Ivan Franko National University of Lviv

Lu Wang

University of Science and Technology of China

Nataliia S. Vorobeva

University of Nebraska–Lincoln, nataliia.vorobeva@huskers.unl.edu

Alexey Lipatov

University of Nebraska-Lincoln, alipatov@unl.edu

*See next page for additional authors*

Follow this and additional works at: <https://digitalcommons.unl.edu/physicsdowben>



Part of the [Atomic, Molecular and Optical Physics Commons](#), [Condensed Matter Physics Commons](#), [Engineering Physics Commons](#), and the [Other Physics Commons](#)

---

Dhingra, Archit; Galiy, Pavlo V.; Wang, Lu; Vorobeva, Nataliia S.; Lipatov, Alexey; Torres, Angel; Nenchuk, Taras M.; Gilbert, Simeon J.; Sinitiskii, Alexander; Yost, Andrew J.; Mei, Wai-Ning; Fukutani, Keisuke; Chen, Jia Shiang; and Dowben, Peter, "Surface termination and Schottky-barrier formation of  $\text{In}_4\text{Se}_3(001)$ " (2020). *Peter Dowben Publications*. 278.

<https://digitalcommons.unl.edu/physicsdowben/278>

This Article is brought to you for free and open access by the Research Papers in Physics and Astronomy at DigitalCommons@University of Nebraska - Lincoln. It has been accepted for inclusion in Peter Dowben Publications by an authorized administrator of DigitalCommons@University of Nebraska - Lincoln.

---

## Authors

Archit Dhingra, Pavlo V. Galiy, Lu Wang, Nataliia S. Vorobeva, Alexey Lipatov, Angel Torres, Taras M. Nenchuk, Simeon J. Gilbert, Alexander Sinitskii, Andrew J. Yost, Wai-Ning Mei, Keisuke Fukutani, Jia Shiang Chen, and Peter Dowben

PAPER

## Surface termination and Schottky-barrier formation of $\text{In}_4\text{Se}_3(001)$

To cite this article: Archit Dhingra *et al* 2020 *Semicond. Sci. Technol.* **35** 065009

### Manuscript version: Accepted Manuscript

Accepted Manuscript is “the version of the article accepted for publication including all changes made as a result of the peer review process, and which may also include the addition to the article by IOP Publishing of a header, an article ID, a cover sheet and/or an ‘Accepted Manuscript’ watermark, but excluding any other editing, typesetting or other changes made by IOP Publishing and/or its licensors”

This Accepted Manuscript is © © 2020 IOP Publishing Ltd.

During the embargo period (the 12 month period from the publication of the Version of Record of this article), the Accepted Manuscript is fully protected by copyright and cannot be reused or reposted elsewhere.

As the Version of Record of this article is going to be / has been published on a subscription basis, this Accepted Manuscript is available for reuse under a CC BY-NC-ND 3.0 licence after the 12 month embargo period.

After the embargo period, everyone is permitted to use copy and redistribute this article for non-commercial purposes only, provided that they adhere to all the terms of the licence <https://creativecommons.org/licenses/by-nc-nd/3.0>

Although reasonable endeavours have been taken to obtain all necessary permissions from third parties to include their copyrighted content within this article, their full citation and copyright line may not be present in this Accepted Manuscript version. Before using any content from this article, please refer to the Version of Record on IOPscience once published for full citation and copyright details, as permissions will likely be required. All third party content is fully copyright protected, unless specifically stated otherwise in the figure caption in the Version of Record.

View the [article online](#) for updates and enhancements.

## Surface Termination and Schottky-Barrier Formation of $\text{In}_4\text{Se}_3(001)$

Archit Dhingra<sup>1</sup>, Pavlo V. Galiy<sup>2</sup>, Lu Wang<sup>3</sup>, Nataliia S. Vorobeva<sup>4</sup>, Alexey Lipatov<sup>4</sup>, Angel Torres,<sup>4</sup> Taras M. Nenchuk<sup>2</sup>, Simeon J. Gilbert<sup>1</sup>, Alexander Sinitskii<sup>4</sup>, Andrew J. Yost<sup>5</sup>, Wai-Ning Mei<sup>6</sup>, Keisuke Fukutani<sup>1</sup>, Jia-Shiang Chen<sup>7</sup> and Peter A. Dowben<sup>1</sup>

<sup>1</sup> Department of Physics and Astronomy, University of Nebraska–Lincoln, Jorgenson Hall, 855 North 16th Street, Lincoln, NE 68588-0299, U. S. A.

<sup>2</sup> Electronics Department, Ivan Franko L'viv National University, L'viv, Ukraine

<sup>3</sup> CAS Key Lab of Materials for Energy Conversion, University of Science and Technology of China, Hefei, China

<sup>4</sup> Department of Chemistry, University of Nebraska–Lincoln, Lincoln, NE 68588, U. S. A.

<sup>5</sup> Department of Physics, Oklahoma State University, Stillwater, OK 74078-3072, U. S. A.

<sup>6</sup> Department of Physics, University of Nebraska - Omaha, Omaha, NE 68182, U. S. A.

<sup>7</sup> Center for Functional Nanomaterials, Brookhaven National Laboratory, Upton, NY 11973, U. S. A.

### Abstract

The surface termination of  $\text{In}_4\text{Se}_3(001)$  and the interface of this layered trichalcogenide, with Au, was examined using X-ray photoemission spectroscopy. Low energy electron diffraction indicates that the surface is highly crystalline, but suggests an absence of  $C_{v2}$  mirror plane symmetry. The surface termination of the  $\text{In}_4\text{Se}_3(001)$  is found, by angle-resolved X-ray photoemission spectroscopy, to be In, which is consistent with the observed Schottky barrier formation found with this n-type semiconductor. Transistor measurements confirm earlier results from photoemission, suggesting that  $\text{In}_4\text{Se}_3(001)$  is n-type semiconductor, so that Schottky barrier formation with a large work function metal, such as Au, is expected. The measured low carrier mobilities could be the result of the contacts and would be consistent with Schottky barrier formation.

**Keywords:** quasi-1D trichalcogenide, surface termination, surface-to-bulk core level shift, Schottky barrier,  $\text{In}_4\text{Se}_3$

## 1. Introduction

Over the past few years, the transition metal trichalcogenides have garnered more and more attention due to the fact that they possess atomically precise 1D chains as their smallest structural unit, which can exist without defects such as dangling bonds or stabilizing functional groups [1–3]. Thus, their edges lack the disorder, prevalent in other systems, such as transition metal dichalcogenides and graphene based materials, which causes unfavorable electronic properties as the channel width decreases [4–10]. As a result, transition metal trichalcogenides, such as  $\text{In}_4\text{Se}_3$ , have great potential for the miniaturization of electronic devices [1,11].  $\text{In}_4\text{Se}_3$  is a semiconductor that forms a layered structure characterized by strong covalent-ionic interactions within the layer but weaker interactions between layers. The (001) surface is not “smooth”, so the layers are not perfectly flat but corrugated [12–19], resulting in quasi-one-dimensional chain structures at the semiconducting  $\text{In}_4\text{Se}_3(001)$  surface.  $\text{In}_4\text{Se}_3$  is, in fact, dominated by  $(\text{In}_3)^{5+}$  multivalent indium bonded with selenium through ionic and covalent bonds.  $\text{In}_4\text{Se}_3$  has a highly anisotropic band structure [16–18], and a direct band gap variously measured to be between 1.1 to 1.3 eV [16–18], making the band gap of  $\text{In}_4\text{Se}_3$  comparable to that of silicon (1.1 eV). Transport measurements place the band gap at a smaller value of about 0.6 eV [19,20]. The placement of the valence band well below the Fermi level, seen in angle resolved valence band photoemission [16–18], suggests an n-type semiconductor, and is consistent with the transistor characteristics [21].

Considerable interest in  $\text{In}_4\text{Se}_3$  has been motivated by its thermoelectric properties [19,22–29]. One key issue with  $\text{In}_4\text{Se}_3$  is that this material is much harder to cleave than materials such as  $\text{TiS}_3$ , and the metal dichalcogenides, which can be mechanically exfoliated with ease, suggesting the adhesion is greater than for  $\text{TiS}_3$  [2]. The higher interlayer adhesion energies, for  $\text{In}_4\text{Se}_3$ , raise questions about the exact nature of the surface termination. Unlike

TiS<sub>3</sub> and the transition metal dichalcogenides, it is less clear that In<sub>4</sub>X<sub>3</sub> (X=S, Se, Te) terminates in the chalcogen. The surface termination matters because the interface and device characteristics depend on the metal to semiconductor interface. Yet little is actually known about the surface termination and the metal-semiconductor interface of semiconducting In<sub>4</sub>Se<sub>3</sub>(001) surface.

In this study, we explored the surface chemistry of the In<sub>4</sub>Se<sub>3</sub>(001) surface through angle resolved X-ray photoemission spectroscopy, and compared experiment to density functional theory calculations.

## 2. Experimental Methods

The In<sub>4</sub>Se<sub>3</sub> crystals were grown by the Czochralski method [17] and then cleaved. The powder diffraction, taken with Cu K $\alpha$ 1 radiation and Reitveld refinement analysis as seen in Figure 1, confirms that the In<sub>4</sub>Se<sub>3</sub> samples are pure and single-phase, with the spatial group Pnnm and lattice constants  $a = 15.290 \text{ \AA}$ ,  $b = 12.307 \text{ \AA}$ ,  $c = 4.081 \text{ \AA}$ , while the volume of the elementary cell is seen to be  $767.88(4) \text{ \AA}^3$ , as expected [12]. The layered crystal structure of In<sub>4</sub>Se<sub>3</sub> allows one to obtain cleaved (001) surfaces [16–18], as schematically indicated in Figure 2. The resulting surface is highly ordered with the correct surface crystal structure, as is evident in low energy electron diffraction, as seen in Figure 3. The cleaved crystals were examined using X-ray photoemission spectroscopy (XPS). The physical evaporation of the Au adlayer onto In<sub>4</sub>Se<sub>3</sub>(001) resulted in Au thicknesses between  $12 \text{ \AA}$  and  $24 \text{ \AA}$ . The thickness of Au adlayers was monitored using a thickness monitor, with the increments in the adlayer thickness being about  $4 \text{ \AA}$ .

The core level X-ray photoemission spectroscopy (XPS) was done using a SPECS X-ray Al anode ( $h\nu = 1486.6$  eV) source and a Phi hemispherical electron analyzer (PHI Model 10-360) with an angular acceptance of  $\pm 10^\circ$  or more. The angle resolved XPS was performed with a VG100AX hemispherical analyzer also using a SPECS X-ray Al anode ( $h\nu = 1486.6$  eV) source. All XPS measurements were undertaken at room temperature in an ultra-high vacuum (UHV) chamber with a base pressure better than  $1 \times 10^{-9}$  mbar.

Electronic transport properties of  $\text{In}_4\text{Se}_3$  were studied using 2- and 4-terminal field-effect transistors (FETs). For the device fabrication, a bulk crystal of  $\text{In}_4\text{Se}_3$  was cleaved using a razor blade, and thin  $\text{In}_4\text{Se}_3$  crystals were pressed onto a heavily p-doped Si substrate covered with a 300-nm-thick layer of  $\text{SiO}_2$ . The heavily p-doped Si substrate served as the bottom gate ( $G$ ) electrode for the electric field-effect measurements. Large and thin  $\text{In}_4\text{Se}_3$  flakes suitable for device fabrication were located using an optical microscope, and electrodes were patterned by standard electron beam lithography (EBL) technique using a Zeiss Supra 40 field-emission scanning electron microscope and a Raith pattern generator. An AJA electron beam evaporation system, at the base pressure of  $\sim 8 \times 10^{-9}$  Torr, was used to complete the electrode fabrication by depositing 2 nm of Cr and 15 nm of Au immediately after the EBL patterning; the Cr sublayer was used to improve the adhesion of gold to the Si/ $\text{SiO}_2$  substrate and the  $\text{In}_4\text{Se}_3$  channel material. In order to examine the morphology of  $\text{In}_4\text{Se}_3$  crystals, in the fabricated devices, we employed atomic force microscopy (AFM), which was performed using a Digital Instruments Nanoscope IIIa Dimension 3100 system. The transport measurements were performed in a Lake Shore TTPX cryogenic probe station at a base pressure of about  $2 \times 10^{-6}$  Torr. The electrical characteristics of the devices were recorded using an Agilent 4155C semiconductor parameter analyzer. A  $4\ \mu\text{m}$  long  $\text{In}_4\text{Se}_3$  phototransistor was created by mechanically exfoliating  $\text{In}_4\text{Se}_3$

flakes onto SiO<sub>2</sub>. Again, electrodes comprised of 5 nm Cr and 45 nm Au were fashioned at the Nebraska Center for Materials and Nanoscience using Heidelberg DWL 66FS laser lithography and AJA electron-beam evaporation systems. Phototransistor measurements were taken at Brookhaven National Lab in the Center for Functional Nanomaterials, with illumination from a 488 nm solid state laser (Coherent Sapphire 100), focused onto the transistor channel using an Olympus IX 81 microscope equipped with a 40×, 0.6 numerical aperture lens.

### 3. Theoretical Methods

The calculations were performed in the framework of density functional theory (DFT) as implemented in the CASTEP code [30]. The plane wave basis set with energy cutoff around 310 eV and ultra-soft pseudopotentials were employed together with the generalized gradient approximation (GGA) in the Perdew–Burke–Ernzerhof (PBE) [31] form for the exchange and correlation functional. Geometry optimizations were performed for the coordinates of the atoms until the maximum force on the atoms was less than 0.03 eV/Å. To understand the stability of the slab surface systems, we calculated the binding energies ( $E_b$ ) of the slabs defined as:  $E_b[\text{Slab}] = E[\text{Slab}] - nE[\text{In}] - mE[\text{Se}]$ , where  $E[\text{Slab}]$  represents the total energy of the slab,  $E[\text{In}]$  and  $E[\text{Se}]$  represent the total energy per atom of In and Se,  $n$  and  $m$  are the numbers of In and Se atoms in the slab.

### 4. Surface Termination

For In<sub>4</sub>Se<sub>3</sub>(100) and In<sub>4</sub>Se<sub>3</sub>(010) only one surface termination was considered in the DFT calculations. For the more facile cleavage plane, In<sub>4</sub>Se<sub>3</sub>(001), surfaces capped with either In



atoms or with Se were considered possible, as indicated in Figure 2. The energies of these various surfaces have been calculated, as summarized in Table 1. The results revealed that, in principle,  $\text{In}_4\text{Se}_3(010)$  is the most stable in terms of binding energy per atom. For the  $\text{In}_4\text{Se}_3(001)$ , the Se surface termination is predicted by DFT to be slightly more stable, in terms of binding energy per atom, than the In terminated surface (Table 1). If, however, the surface terminates in indium, this presents a problem from the point of view of making contacts with low or negligible contact potentials, as the resulting energy barrier would be largely Schottky type. In the case of the  $\text{MX}_3$  (M=Ti, Zr, Hf; X=S, Se, Te) class of metal trichalcogenides [32], specifically  $\text{TiS}_3$ , the strong chemical interactions with the sulfur at the interface with Au and Pt are strong enough to suppress Schottky barrier formation. In the case of  $\text{In}_4\text{Se}_3(100)$  with an In surface termination, strong chemical interactions with the chalcogen (in this case selenium) are far less likely.

The XPS core level features for the In  $3d_{5/2}$  core level contain two components at  $444.5 \pm 0.1$  eV and  $445.4 \pm 0.2$  eV that may be attributed to a surface-to-bulk core level shift in binding energy [33–40] as seen in Figure 4 and Figure 5. As the emission angle increases with respect to the surface normal XPS becomes more sensitive to the surface region. Thus, if there is an increase in intensity, for one of the core level features, it is reasonable to assume that this feature has a stronger presence in the surface region. With increasing emission angle, with respect to the surface normal, the In  $3d_{5/2}$  core level component, at  $444.5 \pm 0.1$  eV, decreases in intensity relative to the In  $3d_{5/2}$  core level component at a binding energy of  $445.4 \pm 0.1$  eV, as seen in Figure 5. Thus, it is appropriate to assign the component at 445.4 eV as a surface feature and the component at 444.5 eV as a bulk feature. This surface-to-bulk core level shift at the In  $3d_{5/2}$  core level, for the  $\text{In}_4\text{Se}_3(001)$  surface, is nearly 1 eV, indicative of a very different

coordination of surface In compared to the bulk. This large surface-to-bulk core level shift suggests two distinct bonding environments for the In atom and the possibility of In surface termination. The bulk In  $3d_{5/2}$  component of  $\text{In}_4\text{Se}_3(001)$ , at  $444.5 \pm 0.1$  eV, is in the region of the 444.7 eV binding energy of  $\text{In}_2\text{S}_3$  [41] and the core level binding energy of 444.47 eV previously reported for  $\text{In}_4\text{Se}_3(001)$  [42]. Indeed, two In  $3d_{5/2}$  core level components, similar to those reported here, were observed in prior X-ray photoemission measurements [42].

The ratio of the relative intensities of the X-ray photoemission spectra for In 3d and Se 3d core level features, with increasing take-off angle with respect to the surface normal, provides a good indication of the surface termination of the  $\text{In}_4\text{Se}_3(001)$  [33,43]. Figure 5 shows Se/In peak intensity ratios, for the Se 3d and In 3d core levels, with respect to the take-off angle. Here, the angle is measured (in degrees) from the normal with respect to the surface of the layered  $\text{In}_4\text{Se}_3(001)$  crystal. The Se/In core level peak intensity ratio drops as the photoelectron emission angle, with respect to the surface normal, increases. As previously mentioned, XPS becomes more surface sensitive as the emission angle with respect to the surface normal increases. As the presence of Se seems to be decreasing with increasing emission angle, it can be inferred that In is more present at the surface than Se. Thus, the variation in Se 3d to In 3d core level photoemission peak intensity ratios, extracted from the angle-resolved XPS (ARXPS) measurements, convincingly indicates that the layered  $\text{In}_4\text{Se}_3(001)$  system terminates in In (and not Se).

If the surface termination results in a polar surface, which cannot be excluded *a priori*, significant reconstructions are then likely, as the surface free energy would be high. Minor reconstructions of the surface are seen in theory, but we have, as yet, no evidence of major surface reconstructions in experiment, as is evident in low energy electron diffraction (LEED), as

seen in Figure 3. Although the crystal structure is nominally orthorhombic, LEED intensity versus voltage analysis of the diffraction beams (Figure 3) indicates that mirror plane symmetry is broken at the (001) surface, so spin-orbit coupling may play a role. The chemical formula is  $\text{In}_4\text{Se}_3$ , so an excess of In at the surface is possible without a net polarization through the crystal, just as a surface dipole occurs in many 2D layered materials ( $\text{MoS}_2$ ,  $\text{WeS}_2$ ,  $\text{TiS}_3$ , etc.).

## 5. Schottky Barrier Formation

A potential barrier for flowing electrons forms at a metal-semiconductor interface, and the type of barrier can be somewhat predicted by the Schottky-Mott model [44,45], which suggests that for high work function metals, such as Au (with work functions of 5.1 eV [46] to 5.4 eV [47]) a Schottky barrier will form when in contact with n-type semiconductors [48]. Although this rule is not always true in experiment, as the chemical reactions at the semiconductor surface tend to govern the resulting interface barrier rather than the work function difference. One example of an exception to the Schottky-Mott rule is another trichalcogenide  $\text{TiS}_3$  [32], where large work function metals such as Au and Pt form an Ohmic contact rather than a Schottky contact. Despite some exceptions, the Schottky barrier formation occurs as a result of upward band bending at the metal-semiconductor interface and has a signature in XPS measurements, as the Schottky barrier formation is accompanied by a shift in the semiconductor's photoemission core level features toward lower binding energies.

Ohmic metallization versus Schottky rectifying behavior of metal contacts at the surface of semiconductors is complicated and depends on many factors such as the type of contact material, the pre- and post-annealing procedures, the number of layers of the contacts (single, bilayer, multilayer), and even the thickness of the layer(s) [49–52]. Au is a widely used materials

for device contacts and Figure 4 shows the evolution of the In  $3d_{5/2}$  core level components, for  $\text{In}_4\text{Se}_3$ , with increasing Au adlayer thickness. In the case of the In  $3d_{5/2}$  surface core level component, there is a clear shift in the observed core level binding energy, with increasing Au coverage on  $\text{In}_4\text{Se}_3(001)$ . The binding energy shift of the In  $3d_{5/2}$  surface core level component is  $\sim 0.58$  eV (Figures 4 and 7). The bulk  $\text{In}_4\text{Se}_3$  In 3d component may also shift to smaller binding energies but not well outside the margin of error. This shift to lower binding energies, in an n-type semiconductor, is very typical of Schottky barrier formation, and indeed is expected [53-58]. The Schottky barrier height, with gold, cannot be less than 0.58 eV, based on the observed In 3d core level shift.

Figure 8a shows the AFM image of the fabricated 4-terminal FET, with an  $\text{In}_4\text{Se}_3$  channel. The parallel lines visible in the device channel are consistent with the quasi-1D chains in the crystal structure of  $\text{In}_4\text{Se}_3$ ; similar observations were previously made in the AFM studies of other quasi-1D materials, such as  $\text{TiS}_3$  [2]. The  $V_1$  and  $V_2$  electrodes were used either as voltage probes in the 4-terminal measurements or as drain and source electrodes in the 2-terminal measurements. According to the AFM image, the channel's length between the  $V_1$  and  $V_2$  electrodes was about  $1.9 \mu\text{m}$  while its width was about  $9.8 \mu\text{m}$ . The height of  $\text{In}_4\text{Se}_3$  varied significantly from 5 nm at the thinner parts of the flake to up to 40 nm in the center.

Figure 8b presents the results of electric field-effect measurements of the  $\text{In}_4\text{Se}_3$  device in the 2- and 4-terminal configurations. The transistors, with  $\text{In}_4\text{Se}_3$  as the semiconductor channel, show increasing currents with positive gate voltage and increasing resistance with negative gate voltage, as seen in Figure 8b. This is characteristic of an n-type semiconductor and consistent with the observation that the binding energy of the top of the valence band, as seen in photoemission [16–18,59], is very similar to the band gap. This places the conduction band

minimum close to the Fermi level [18,59]. The mobilities of the majority carriers in  $\text{In}_4\text{Se}_3$  transistors fabricated and tested in this study were very low. The mobility measured for the best device was about  $1.5 \text{ cm}^2\text{V}^{-1}\text{s}^{-1}$ , suggesting phonon scattering, as has been seen for  $\text{TiS}_3$  [60], a large effective carrier mass, or contact issues such as Schottky barrier contacts. The electron effective mass cannot be excessively large, judging from the calculated band structure, as plotted in Figure 9 for both the In and Se surface termination. Furthermore, the measured effective electron carrier mass is  $0.16 \pm 0.03 m_e$ , as determined from an experimental band mapping [59]. Such a small measured effective mass suggests this is not the origin of the low measured mobility. We note in passing that the band structure calculations indicate that the effective mass, at the conduction band minimum of the  $\text{In}_4\text{Se}_3(001)$  surface, is either 0.42 or 0.06 that of the free electron mass, with In and Se surface termination respectively.

In the 4-terminal measurements, the channel resistance at  $V_G = 0$  was  $R_{4T} = 33.4 \text{ M}\Omega$ , which translates into the sheet resistance of  $\text{In}_4\text{Se}_3$  along the direction of the quasi-1D chains of  $172 \text{ M}\Omega/\square$ . The difference between the values of 2- and 4-terminal resistances allows an estimation of the contact resistance between  $\text{In}_4\text{Se}_3$  and the Cr/Au contacts. The difference was found to be  $6.7 \text{ M}\Omega$  at  $V_G = 0$ . This value, multiplied by the channel's width and divided by two (for each electrode), translates into a contact resistance of  $R_c = 32.8 \text{ M}\Omega \cdot \mu\text{m}$ . The large contact resistance in this device also manifests in the nonlinear  $I$ - $V$  curves measured for the central segment of the device in the 2-terminal configuration (Figure 8c and Figure 10). The nonlinear current *versus* voltage behavior was observed at all gate voltages, which ranged from -80 to 80 V, and is consistent with Schottky barriers at the device contacts. Because of the Cr (in the Cr/Au) these contacts are not directly comparable to Au alone. As Cr has a work function far

lower than Au, as the work function of Cr = 4.5 eV [46], this means that Cr/Au contacts should be far more ohmic than Au alone.

This nonlinear I(V) behavior, seen at the smaller biases in the two terminal devices, is also present under illumination at photon energies well above the band gap (2.5 eV versus 1.1 eV), as seen in Figure 10, suggesting that hot electron transport does not completely overcome the Schottky barrier. The increased current *versus* voltage, under 2.5 eV photon energy illumination (Figure 10), suggests a significant on/off ratio for In<sub>4</sub>Se<sub>3</sub> as a phototransistor.

## 6. Conclusion

In summary, experiment provides clear indications that In<sub>4</sub>Se<sub>3</sub>(001) is indium surface terminated, defying the expectations of some ground state density functional theory. Future density functional theory should perhaps include an investigation of the dependence of the band structure and the surface free energy *versus* thickness of slab, with and without spin-orbit coupling. The In<sub>4</sub>Se<sub>3</sub>(001) to Au interface appears to result in Schottky barrier formation, suggesting that for better device performance lower work function metals will need to be sought as metal contacts, with the challenge of ensuring that the metal contacts do not form delta doping layers within the In<sub>4</sub>Se<sub>3</sub>(001). The measured low carrier mobilities could be the result of the contacts, and the low mobilities observed are consistent with Schottky barrier formation, but a reduction of carrier mobility due to phonon scattering cannot be excluded from the data. We have good reason to believe that a phototransistor from In<sub>4</sub>Se<sub>3</sub> is possible, so sensing and logic could potentially be integrated. This could be important for robotics applications, if the device physics issues are addressed.

## **Acknowledgments**

This research was supported by the National Science Foundation (NSF), through grants NSF-ECCS 1740136, as well as by the nCORE, a wholly owned subsidiary of the Semiconductor Research Corporation (SRC), through the Center on Antiferromagnetic Magneto-electric Memory and Logic task #2760.002. The research was performed in part in the Nebraska Nanoscale Facility: National Nanotechnology Coordinated Infrastructure and the Nebraska Center for Materials and Nanoscience, which are supported by the National Science Foundation under Award ECCS: 1542182, and the Nebraska Research Initiative. This research used resources of the Center for Functional Nanomaterials, which is a U.S. DOE Office of Science Facility, at Brookhaven National Laboratory under Contract No. DE-SC0012704. The authors acknowledge helpful discussions with Duy Le and Talat Rahman.

## References

- [1] Lipatov A, Wilson P M, Shekhirev M, Teeter J D, Netusil R and Sinitskii A 2015 Few-layered titanium trisulfide ( $\text{TiS}_3$ ) field-effect transistors *Nanoscale* **7** 12291–6
- [2] Lipatov A *et al.* 2018 Quasi-1D  $\text{TiS}_3$  Nanoribbons: Mechanical Exfoliation and Thickness-Dependent Raman Spectroscopy *ACS Nano* **12** 12713–20
- [3] Dai J and Zeng X C 2015 Titanium trisulfide monolayer: Theoretical prediction of a new direct-gap semiconductor with high and anisotropic carrier mobility *Angew. Chem. Int. Edit.* **54** 7572–6
- [4] Dubois S M M, Lopez-Bezanilla A, Cresti A, Triozon F, Biel B, Charlier J C and Roche S 2010 Quantum transport in graphene nanoribbons: Effects of edge reconstruction and chemical reactivity *ACS Nano* **4** 1971–6
- [5] Jensen S A, Ulbricht R, Narita A, Feng X, Müllen K, Hertel T, Turchinovich D and Bonn M 2013 Ultrafast photoconductivity of graphene nanoribbons and carbon nanotubes *Nano Lett.* **13** 5925–30
- [6] Kumar P, Skomski R, Manchanda P, Kashyap A and Dowben P A 2014 Effective mass and band gap of strained graphene *Curr. Appl. Phys.* **14** S136–9
- [7] Baringhaus J *et al.* 2014 Exceptional ballistic transport in epitaxial graphene nanoribbons *Nature* **506** 349–54
- [8] Wimmer M, Adagideli I, Berber S, Tomanek D and Richter K 2008 Spin currents in rough graphene nanoribbons: Universal fluctuations and spin injection *Phys. Rev. Lett.* **100** 3–6
- [9] Han M Y, Brant J C and Kim P 2010 Electron transport in disordered graphene nanoribbons *Phys. Rev. Lett.* **104** 056801
- [10] Wang X, Ouyang Y, Jiao L, Wang H, Xie L, Wu J, Guo J and Dai H 2011 Graphene nanoribbons with smooth edges behave as quantum wires *Nat. Nanotechnol.* **6** 563–7
- [11] Island J O, Buscema M, Barawi M, Clamagirand J M, Ares J R, Sánchez C, Ferrer I J, Steele G A, van der Zant H S J and Castellanos-Gomez A 2014 Ultrahigh photoresponse of few-layer  $\text{TiS}_3$  nanoribbon transistors *Adv. Opt. Mater.* **2** 641–5
- [12] Hogg J H C, Sutherland H H and Williams D J 1973 The crystal structure of tetraindium triselenide *Acta Crystallogr. B* 1590–3
- [13] Likfomann A and Eitienne J 1972 Crystalline-Structure of Indium-4 Selenium-3 *C. R. Acad. Sci. C* **275** 1097
- [14] Man L I, Imamov R M and Semiletov S A 1976 Types of crystal structures of the Ga, In and Tl chalcogenides *Kristallografiya* **21** 628–39
- [15] Schwarz U, Hillebrecht H, Deiseroth H J and Walther R 1995  $\text{In}_4\text{Te}_3$  und  $\text{In}_4\text{Se}_3$ : Neubestimmung der Kristallstrukturen, druckabhängiges Verhalten und eine Bemerkung zur Nichtexistenz von  $\text{In}_4\text{S}_3$  *Z. Kristallogr.* **210** 342–7



- [16] Losovyj Y B *et al.* 2008 The electronic structure of surface chains in the layered semiconductor  $\text{In}_4\text{Se}_3(100)$  *Appl. Phys. Lett.* **92** 122107
- [17] Losovyj Y B, Makinistian L, Albanesi E A, Petukhov A G, Liu J, Galiy P, Dveriy O R and Dowben P A 2008 The anisotropic band structure of layered  $\text{In}_4\text{Se}_3(001)$  *J. Appl. Phys.* **104** 083713
- [18] Fukutani K, Miyata Y, Matsuzaki I, Galiy P V, Dowben P A, Sato T and Takahashi T 2015 High-resolution angle-resolved photoemission study of quasi-one-dimensional semiconductor  $\text{In}_4\text{Se}_3$  *J. Phys. Soc. Jpn.* **84** 1–6
- [19] Lim Y S, Jeong M, Seo W S, Lee J H, Park C H, Sznajder M, Kharkhalis L Y, Bercha D M and Yang J 2013 Condensation state and its effects on thermoelectric properties in  $\text{In}_4\text{Se}_3$  *J. Phys. D Appl. Phys.* **46** 275304
- [20] Bercha D M, Mitin O B, Kharkhalis L Yu and Bercha A I 1995 Properties of the band structure of  $\text{In}_4\text{Se}_3$  crystals *Phys. Solid State* **37** 1778-81
- [21] Galiy P V *et al.* 2019 Building the Quasi One Dimensional Transistor from 2D Materials 2019 *IEEE 2nd Ukraine Conference on Electrical and Computer Engineering, IEEE Xplore* pp 679–82
- [22] Rhyee J S, Lee K H, Lee S M, Cho E, Kim S Il, Lee E, Kwon Y S, Shim J H and Kotliar G 2009 Peierls distortion as a route to high thermoelectric performance in  $\text{In}_4\text{Se}_3$  crystals *Nature* **459** 965–8
- [23] Shi X, Cho J Y, Salvador J R, Yang J and Wang H 2010 Thermoelectric properties of polycrystalline  $\text{In}_4\text{Se}_3$  and  $\text{In}_4\text{Te}_3$  *Appl. Phys. Lett.* **96** 162108
- [24] Rhyee J S, Ahn K, Lee K H, Ji H S and Shim J H 2011 Enhancement of the thermoelectric figure-of-merit in a wide temperature range in  $\text{In}_4\text{Se}_{3-x}\text{Cl}_{0.03}$  bulk crystals *Adv. Mater.* **23** 2191–4
- [25] Zhu G H, Lan Y C, Wang H, Joshi G, Hao Q, Chen G and Ren Z F 2011 Effect of selenium deficiency on the thermoelectric properties of n-type  $\text{In}_4\text{Se}_{3-x}$  compounds *Phys. Rev. B* **83** 3–6
- [26] Lim Y S, Cho J Y, Lee J K, Choi S M, Kim K H, Seo W S and Park H H 2010 Microstructures and thermoelectric properties of spark plasma sintered  $\text{In}_4\text{Se}_3$  *Electron. Mater. Lett.* **6** 117–21
- [27] Rhyee J-S, Cho E, Lee K H, Lee S M, Kim S Il, Kim H-S, Kwon Y S and Kim S J 2009 Thermoelectric properties and anisotropic electronic band structure on the  $\text{In}_4\text{Se}_{3-x}$  compounds *Appl. Phys. Lett.* **95** 212106
- [28] Yin X, Liu J-Y, Chen L and Wu L-M 2018 High Thermoelectric Performance of  $\text{In}_4\text{Se}_3$ -Based Materials and the Influencing Factors *Accounts Chem. Res.* **51** 240–7
- [29] Chen Y-C, Lin H and Wu L-M 2016 High thermoelectric performance of polycrystalline  $\text{In}_4\text{Se}_{3-\delta}(\text{CuI})_x$ : synergistic effects of the Se-deficiency and CuI-doping *Inorg. Chem. Front.* **3** 1566–71

- [30] Segall M D, Lindan P J D, Probert M J, Pickard C J, Hasnip P J, Clark S J and Payne M C 2002 First-principles simulation: Ideas, illustrations and the CASTEP code *J. Phys. Condens. Mat.* **14** 2717–44
- [31] Perdew J P, Burke K and Ernzerhof M 1996 Generalized gradient approximation made simple *Phys. Rev. Lett.* **77** 3865–8
- [32] Gilbert S J, Lipatov A, Yost A J, Loes M J, Sinitskii A and Dowben P A 2019 The electronic properties of Au and Pt metal contacts on quasi-one-dimensional layered  $\text{TiS}_3(001)$  *Appl. Phys. Lett.* **114** 101604
- [33] Egelhoff W F 1987 Core-level binding-energy shifts at surfaces and in solids *Surf. Sci. Rep.* **6** 253–415
- [34] Spanjaard D, Guillot C, Desjonqueres M C and Treglia G L J 1985 Surface Core Level Spectroscopy of Transition Metals: A New Tool for the Determination of Their Surface Structure *Surf. Sci. Rep.* **5** 1–85
- [35] Desjonqueres M C, Spanjaard D, Lassailly Y and Guillot C 1980 On the origin of the variation of the binding energy shifts of core levels between surface and bulk atoms in transition metals *Solid State Commun.* **34** 807–10
- [36] Rosengren A and Johansson B 1981 Surface heat of segregation from surface core-level binding-energy shifts *Phys. Rev. B* **23** 3852–8
- [37] van der Veen J F, Himpsel F J and Eastman D E 1980 Structure-Dependent 4f —Core-Level Binding Energies for Surface Atoms on Ir(111), Ir(100)-(5 × 1), and Metastable Ir(100)-(1 × 1) *Phys. Rev. Lett.* **44** 189–92
- [38] van der Veen J F, Eastman D E, Bradshaw A M and Holloway S 1981 Intrinsic step-related surface states and 4f-core levels on Ir(332) *Solid State Commun.* **39** 1301–4
- [39] Bartynski R A, Heskett D, Garrison K, Watson G M, Zehner D M, Mei W N, Tong S Y and Pan X 1989 Photoelectron diffraction determination of the geometry of a clean metal surface: Ta(100) *Phys. Rev. B* **40** 5340–3
- [40] Kim B, Chen J, Erskine J L, Mei W N and Wei C M 1993 Surface and bulk photoelectron diffraction from W(110) 4 f core levels *Phys. Rev. B* **48** 4735–40
- [41] Wagner C D, Gale L H and Raymond R H 1979 Two-Dimensional Chemical State Plots: a Standardized Data Set for Use in Identifying Chemical States By X-Ray Photoelectron Spectroscopy *Anal. Chem.* **51** 466–82
- [42] Balitskii O A, Savchyn V P, Jaeckel B and Jaegermann W 2004 Surface characterization of  $\text{In}_4\text{Se}_3$  single crystals *Physica E* **22** 921 – 923
- [43] Dowben P A 1990 Core Level Spectroscopy and the Characterization of Surface Segregation *Surface Segregation Phenomena*
- [44] Schottky W 1939 Zur Halbleitertheorie der Sperrschicht- und Spitzengleichrichter *Z. Phys.* **113** 367–414
- [45] Mott N F 1939 The theory of crystal rectifiers *Proc. R. Soc. A* **171** 153–65

- [46] Eastman D E 1970 Photoelectric work functions of transition, rare-earth, and noble metals *Phys. Rev. B* **2** 1–2
- [47] Potter H C and Blakely J M 1975 LEED, Auger spectroscopy, and contact potential studies of copper–gold alloy single crystal surfaces *J. Vac. Sci. Technol.* **12** 635–42
- [48] Zhang Z and Yates J T 2012 Band Bending in Semiconductors: Chemical and Physical Consequences at Surfaces and Interfaces *Chem. Rev.* **112** 5520–51
- [49] Kurimoto M, Ashrafi A B M A, Ebihara M, Uesugi K, Kumano H and Suemune I 2004 Formation of ohmic contacts to p-type ZnO *Phys. Status Solidi B* **241** 635–9
- [50] Ryu Y R, Lee T S, Leem J H and White H W 2003 Fabrication of homostructural ZnO p–n junctions and ohmic contacts to arsenic-doped p-type ZnO *Appl. Phys. Lett.* **83** 4032–4
- [51] Lee J-M, Kim K-K, Tampo H, Yamada A and Niki S 2006 Ohmic Contact Behavior of Pt/Ni/Au to p-ZnO *MRS Proceedings* **928** 0928–GG09-12
- [52] Brillson L J and Lu Y 2011 ZnO Schottky barriers and Ohmic contacts *J. Appl. Phys.* **109** 121301
- [53] S.R. McHale, J.W. McClory, J.C. Petrosky, J. Wu, A. Rivera, R. Palai, Ya.B. Losovyj, and P.A. Dowben, “Schottky barrier formation at the Au to rare earth doped GaN thin film interface”, *Eur. Phys. J-Appl. Phys* **55** (2011) 31301
- [54] Wu C I and Kahn A 1998, *J. Vac. Sci. Technol. B* **16** 2218
- [55] Barinov A, Casalis L, Gregoratti L and Kiskinova M 2001 *Phys. Rev. B* **63** 85308
- [56] Barinov A, Casalis L, Gregoratti L and Kiskinova M 2001 *J. Phys. D: Appl. Phys.* **34**, 279
- [57] Kim M H, Lee S N, Huh C, Park S Y, Han J Y, Seo J M and Park S J 2000 *Phys. Rev. B* **61** 10966
- [58] Lay G L, Mao D, Kahn A, Hwu Y and Margaritondo G 1991 *Phys. Rev. B* **43** 14301
- [59] Fukutani K, Sato T, Galiy P V, Sugawara K and Takahashi T 2016 Tunable two-dimensional electron gas at the surface of thermoelectric material In<sub>4</sub>Se<sub>3</sub> *Phys. Rev. B* **93** 205156
- [60] Randle M *et al.* 2019 Gate-Controlled Metal–Insulator Transition in TiS<sub>3</sub> Nanowire Field-Effect Transistors *ACS Nano* **13** 803–11

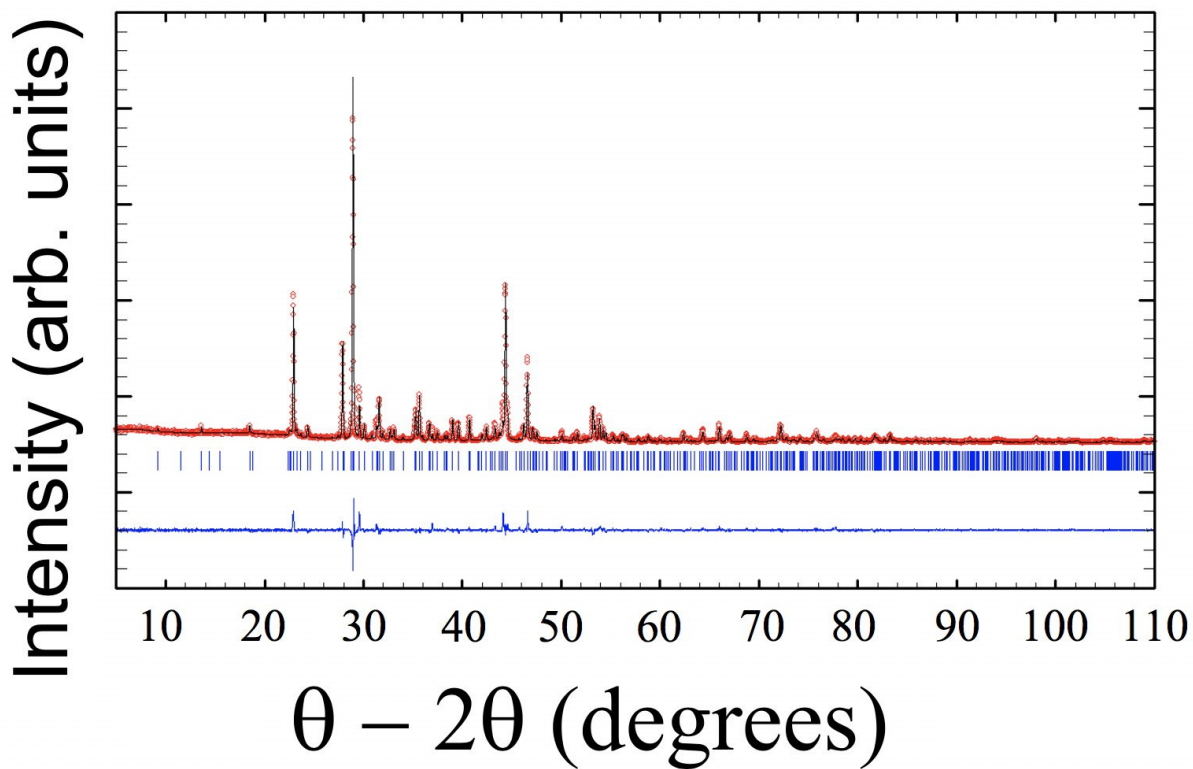


**Figure 1.** The experimental powder X-ray diffraction (rings, red), theoretical fit (solid line, black) and difference (bottom, blue) for  $\text{In}_4\text{Se}_3$ . The Bragg angles (vertical bars) for  $\text{In}_4\text{Se}_3$  of spatial group Pnmm  $a = 15.2902$  (4),  $b = 12.3069$  (3),  $c = 4.08065$  (10) Å, are indicated by the vertical bars.

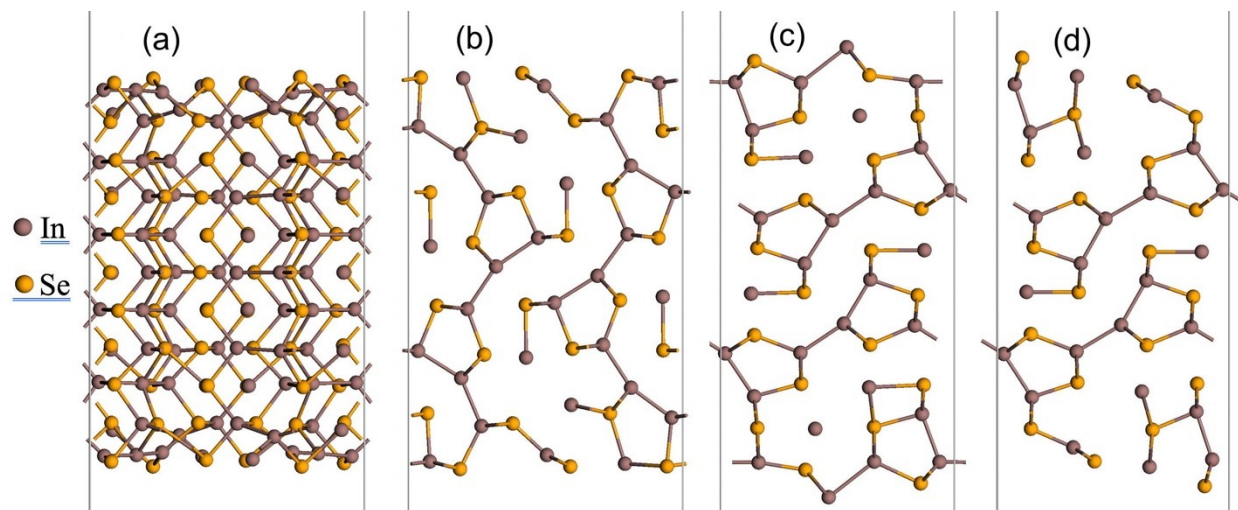


**Figure 2.** The optimized structures of  $\text{In}_4\text{Se}_3$  surface slabs. (a)  $\text{In}_4\text{Se}_3(100)$ , (b)  $\text{In}_4\text{Se}_3(010)$ , (c)  $\text{In}_4\text{Se}_3(001)$  with an In surface termination, (d)  $\text{In}_4\text{Se}_3(001)$  with a Se surface termination.

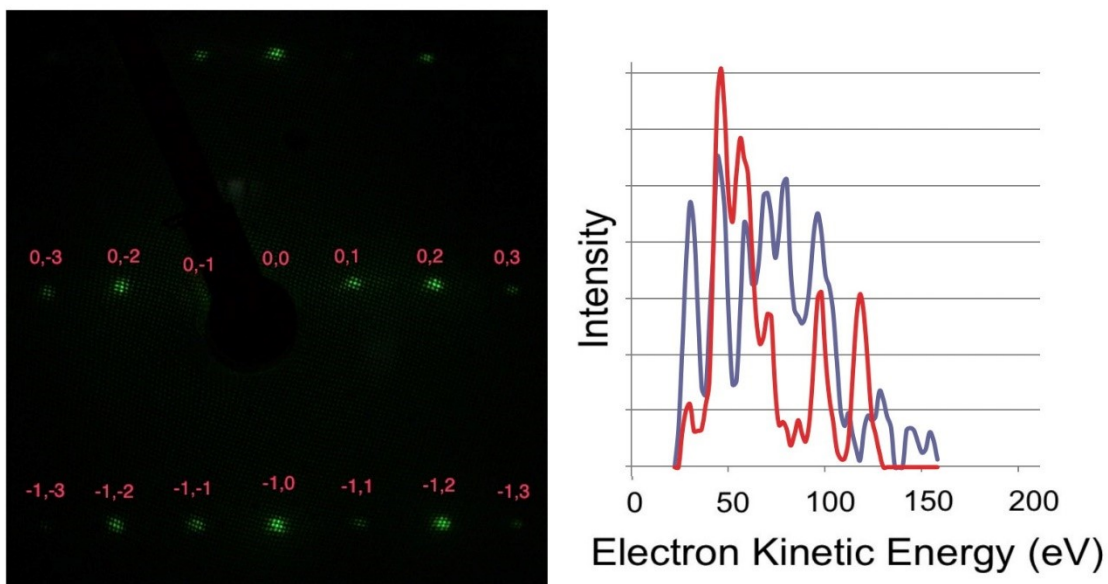


**Figure 3.** The surface crystallography for cleaved  $\text{In}_4\text{Se}_3(001)$  surface, from low energy electron diffraction (LEED, at left). The electron beam energy for LEED is 60 eV. The intensity versus electron kinetic energy,  $I(V)$ , have been plotted, for the 0,-2 (blue) and 0,2 (red) LEED diffraction beams at the right, as indexed in the LEED image (left).

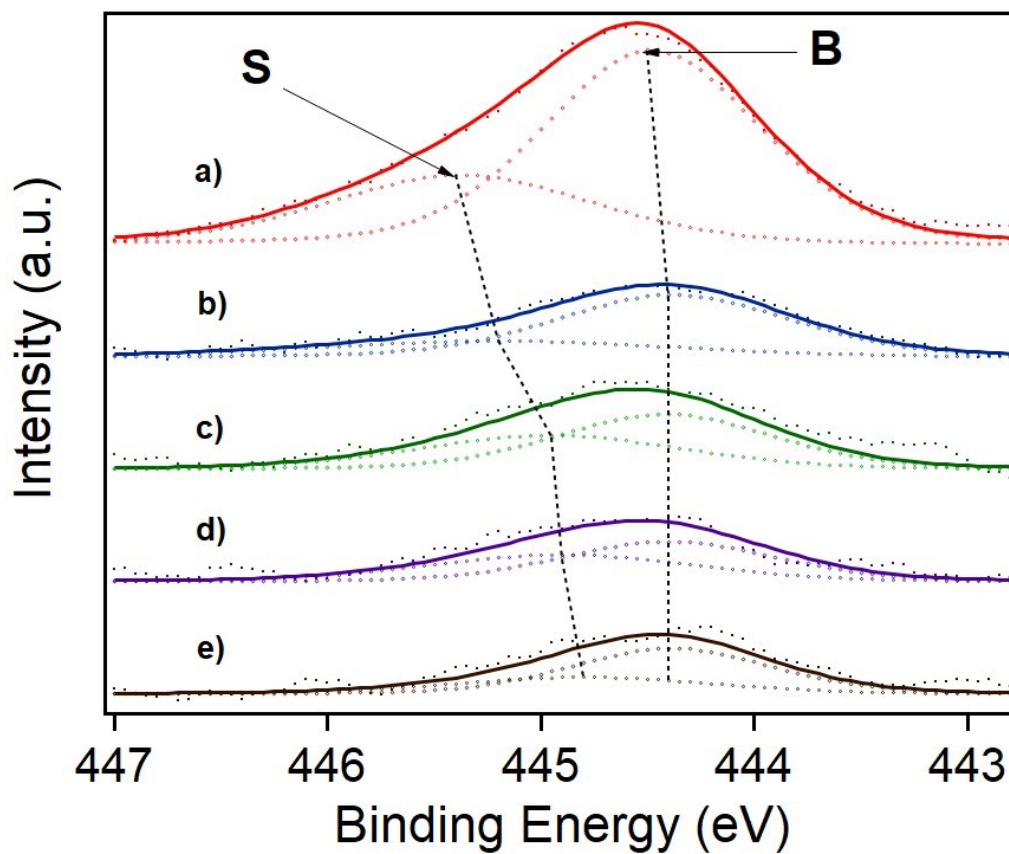


**Figure 4:** The X-ray photoemission spectra of the In 3d<sub>5/2</sub> core level feature of In<sub>4</sub>Se<sub>3</sub> (001) crystal, with increasing Au coverage: a) 0 nm Au, b) 1.2 nm of Au, c) 1.6 nm of Au, d) 2.0 nm of Au and e) 2.4 nm of Au. The dashed lines denote binding energies of the surface (S) and bulk (B) In 3d<sub>5/2</sub> core level components.

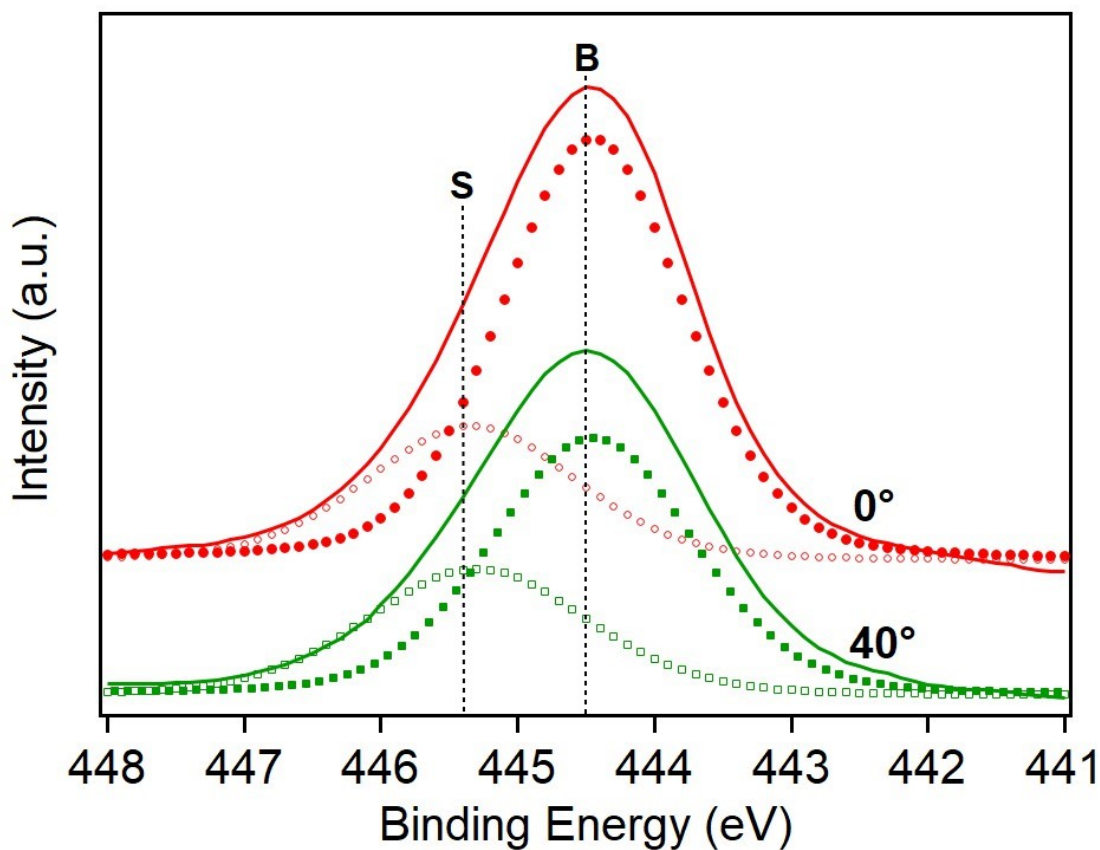


**Figure 5:** The angle-resolved X-ray photoemission spectroscopy (ARXPS) data for In 3d<sub>5/2</sub> core levels with different take-off angles (0° and 40°). Solid lines represent raw data, whereas solid markers represent In<sub>2</sub> 3d<sub>5/2</sub> core level component with bulk (B) weight while hollow markers represent the In<sub>1</sub> 3d<sub>5/2</sub> core level component with surface (S) weight.



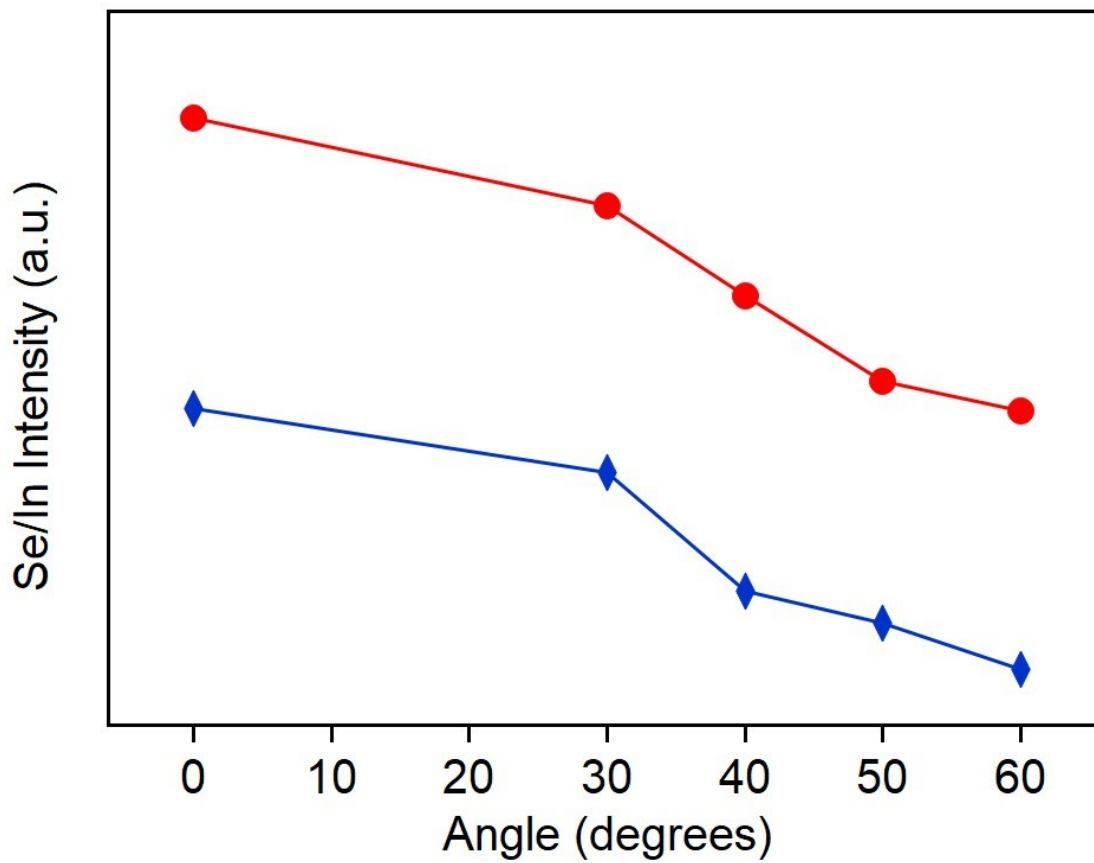


**Figure 6:** The angle-resolved X-ray photoemission spectroscopy (ARXPS) data for photoemission Se/In peak intensity ratios, for core level Se  $3d_{5/2}$  versus In  $3d_{5/2}$  intensities (blue (diamonds)) and Se  $3d_{3/2}$  and In  $3d_{3/2}$  (red (circles)), as a function of the photoemission take-off angle, with respect to the surface normal.

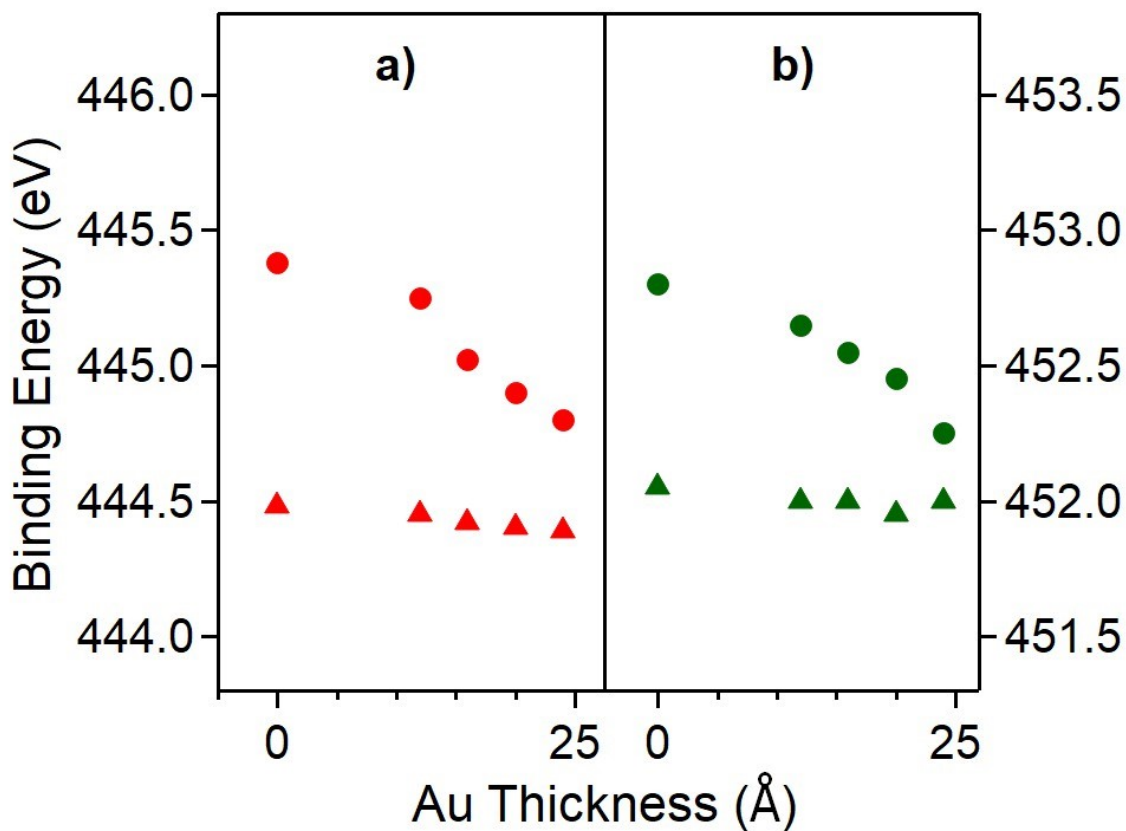


**Figure 7:** The change in (a) In  $3d_{5/2}$  and (b) In  $3d_{3/2}$  core level binding energies, as measured in XPS, for  $\text{In}_4\text{Se}_3$  (001) surface with increasing Au coverage. Circles depict surface In<sub>1</sub> component (indium nearest to the interface), whereas triangles represent the bulk In<sub>2</sub> component (indium away from the interface).

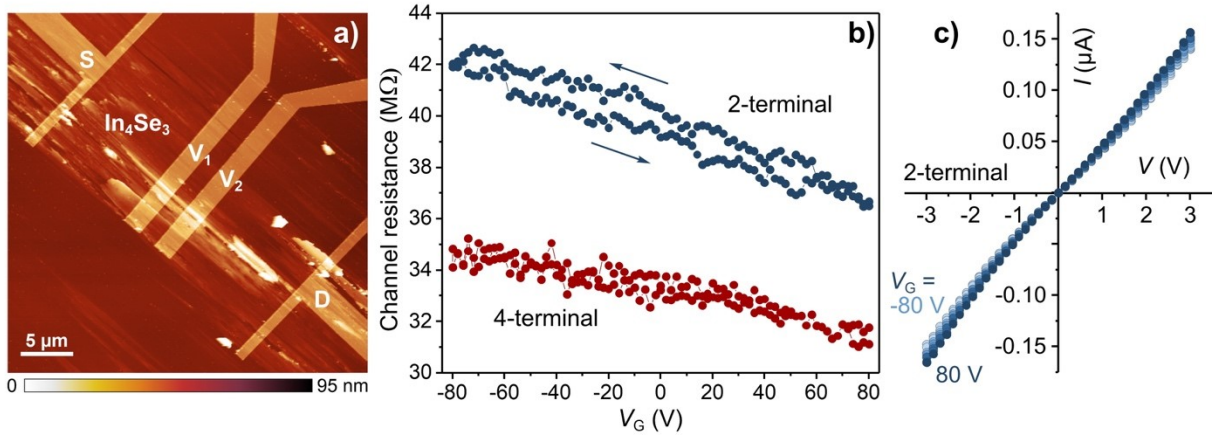


**Figure 8:** Transport properties of  $\text{In}_4\text{Se}_3$  devices. (a) AFM image of a 4-terminal  $\text{In}_4\text{Se}_3$  device with Cr/Au electrodes. The measurements in panels b and c were performed on the central segment of the device between the  $V_1$  and  $V_2$  voltage probes. (b) The dependencies of the resistance of the central device segment on the gate voltage ( $V_G$ ) measured in both 2-terminal (blue) and 4-terminal (red) configurations. (c)  $I$ - $V$  curves obtained by 2-terminal measurements of the central device segment at  $V_G$  ranging from -80 to 80 V.

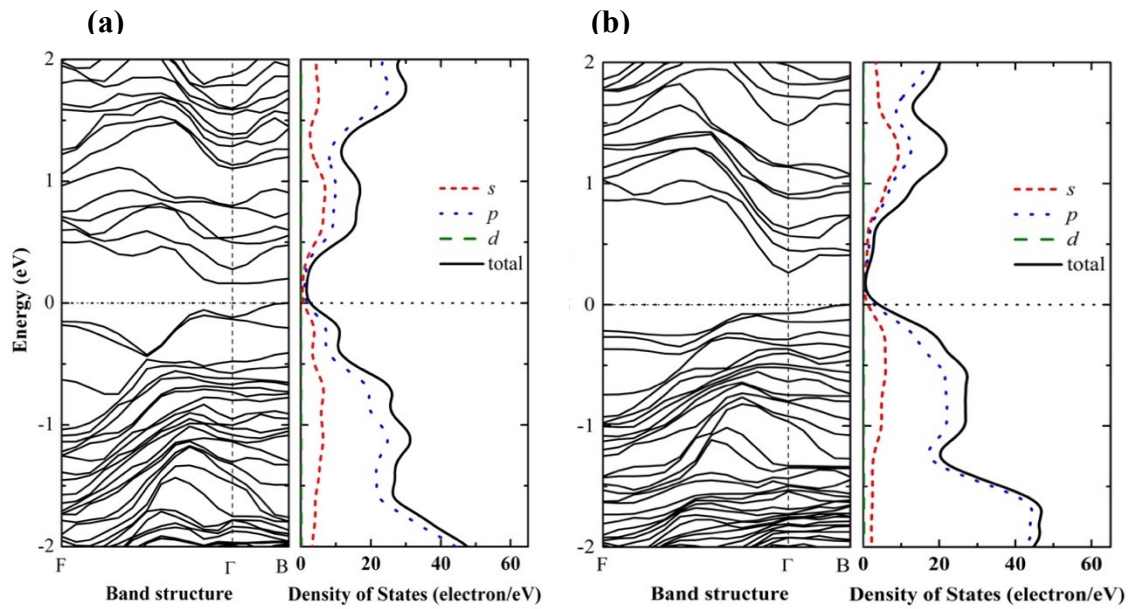


**Figure 9:** The band structure of the  $\text{In}_4\text{Se}_3$  (001) surface with (a) In and (b) Se surface termination. F represents (0.0, 0.5), B represents (0.5, 0.0), and  $\Gamma$  represents (0.0, 0.0) in the two-dimensional Brillouin zone of the surface slabs.

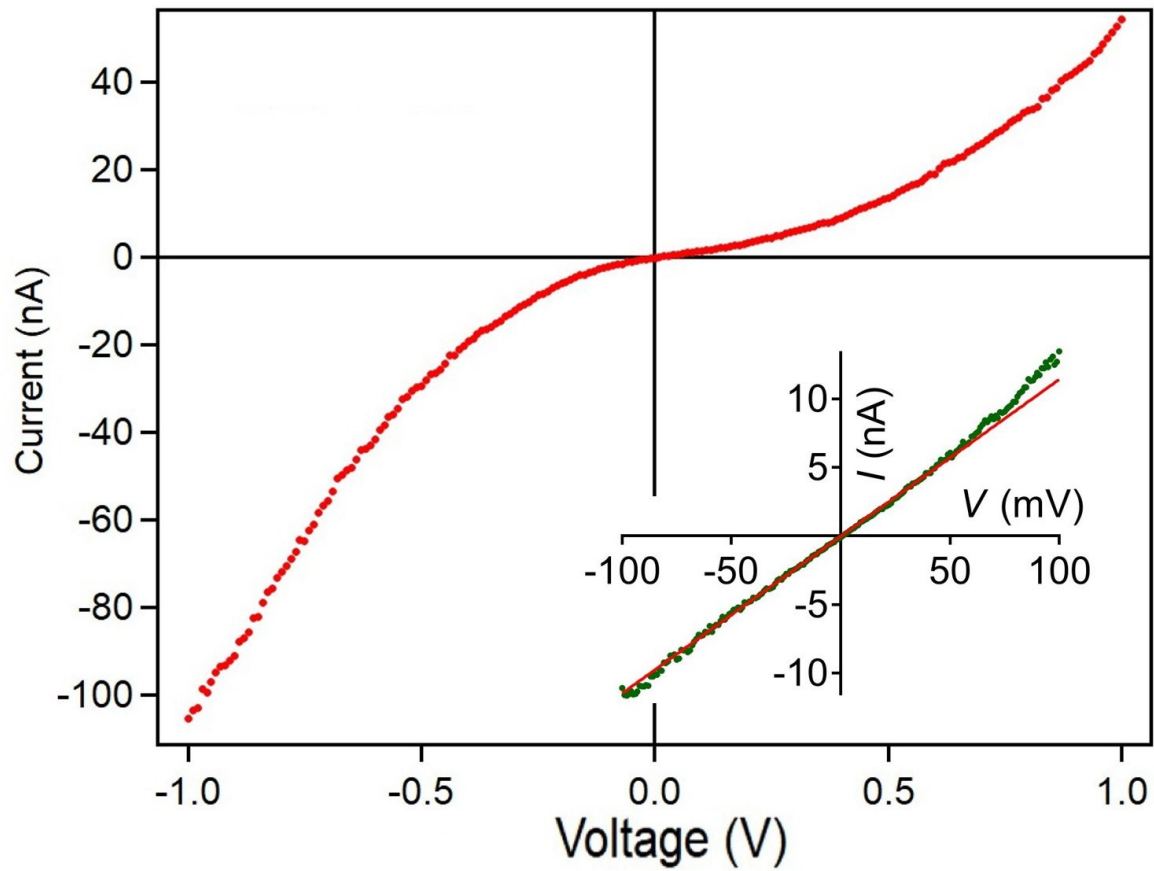


**Figure 10:** Transport properties of a 2 terminal  $\text{In}_4\text{Se}_3$  devices, 20 to 40 nm thick on  $\text{SiO}_2$ , showing nonlinear behavior under no illumination, and retention of some non-linear behavior under  $10 \mu\text{W}$  illumination at 488 nm (roughly 2.5 eV).

Table 1

<b>Calculated binding energies of the In<sub>4</sub>Se<sub>3</sub> surface slabs.</b>				
<i>Slab</i>	<i>n</i>	<i>m</i>	<i>Binding energy (eV)</i>	<i>Binding energy per atom (eV)</i>
In <sub>4</sub> Se <sub>3</sub> (100)	88	66	-58.34	-0.379
In <sub>4</sub> Se <sub>3</sub> (010)	30	24	-22.22	-0.412
In <sub>4</sub> Se <sub>3</sub> (001) In capped	28	20	-18.61	-0.388
In <sub>4</sub> Se <sub>3</sub> (001) Se capped	24	20	-17.32	-0.394